Peer-reviewed version available at Materials 2019, 13, 40; doi:10.3390/ma13010040

Article

Effect of Different Composition on Voltage Attenuation of Li-Rich Cathode Material for Lithium-ion Batteries

Jun Liu [1], Qiming Liu [1], Huali Zhu [2], Feng Lin [1], Yan Ji [1], Bingjing Li [1], Junfei Duan [1], Lingjun Li [1] and Zhaoyong Chen [1,*]

[1] College of Materials Science and Engineering, Changsha University of Science and Technology, Changsha 410114, China; 1948810556@qq.com (J.L.).
[2] College of Physics and Electronic Science, Changsha University of Science and Technology, Changsha, China 410114.
* Correspondence: chenzhaoyongcioc@126.com (Z.C.).

Abstract: Li-rich layered oxide cathode materials have become one of the most promising cathode materials for high-energy-density lithium-ion batteries owning to its high theoretical specific capacity, low cost, high operating voltage and environmental friendliness. Yet they suffer from severe capacity and voltage attenuation during prolong cycling, which blocks their commercial application. To clarify these causes, we synthesize $0.5Li_2MnO_3{\cdot}0.5LiNi_{0.8}Co_{0.1}Mn_{0.1}O_2$ (LL-811) with high-nickel-content cathode material by a solid-sate complexation method, and it manifests a lot slower capacity and voltage attenuation during prolong cycling compared to LL-111 and LL-523 cathode materials. The capacity retention at 1C after 100 cycles reaches to 87.5% and the voltage attenuation after 100 cycles is only 0.460 V. Combining X-ray diffraction (XRD), scanning electron microscope (SEM) and transmission electron microscopy (TEM), it indicates that increasing the nickel content not only stabilizes the structure but also alleviates the attenuation of capacity and voltage. Therefore, it provides a new idea for designing of Li-rich layered oxide cathode materials that suppress voltage and capacity attenuation.

Keywords: Li-rich layered oxide; cathode materials; voltage attenuation; lithium-ion batteries; solid-state complexation method

1. Introduction

Advanced lithium-ion batteries (LIBs) technology have promoted the rapid development of mobile electronic devices owning to their low cost, long life, lack of any memory effect and environmental friendliness [1-3]. The development of hybrid electric vehicles (HEVs) and electric vehicles (EVs) puts higher demands on energy density and cruising range [4-6]. Compared to traditional cathode materials, such as $LiCoO_2$ [7-8], spinel $LiMn_2O_4$ [9-10], polyanionic $LiFePO_4$ [11-12] and layered cathode materials $LiMO_2$ [13-16] (M=Ni, Co, Mn), Li-rich layered oxide cathode materials, represented by the chemical formula $xLi_2MnO_3{\cdot}(1-x)LiMO_2$ ($0 < x < 1$, M = Ni, Co, Mn) have received extensive attention from scientists all over the world because they exhibit a reversible capacity exceeding 250 $mAh{\cdot}g^{-1}$ between 2 V and 4.8 V, as well as their low cost and high energy density (>900 $Wh{\cdot}Kg^{-1}$) [17-18]. Unfortunately, these cathode materials put up with poor kinetics [19] and severe voltage attenuation [20-22] during prolong cycling, which directly affects their electrochemical performance, particularly the energy that the battery can output [23-25]. These disadvantages hinder the commercial development of high-energy-density lithium-ion batteries.

In order to explore effective ways to alleviate the voltage attenuation of Li-rich cathode materials, scientists have done a lot of research work to identify the origin [6,26-28]. The cause of voltage attenuation is generally attributed to a continuous phase transition from layered phase to spinel during the repeated extraction/insertion processes [19,21,29], corresponding to the irreversible migration of the transition metal (TM) ions, during the course of which they move from the octahedral sites in the TM slab to the octahedral sites in the Li slab during the lithium ion extraction/insertion processes [30]. It is possible for Li-rich layered oxide cathode materials to prevent collapse of the layered structure by minimizing the tension between the neighboring oxygen layers in its deep delithiation state. Increasing the nickel content can effectively suppress the voltage attenuation in these cobalt-free or high-nickel cathode materials, which is the development trend of lithium-ion batteries in the future [23,25,31]. Dahn et al. report Core−shell (CS) materials allow that the Mn-rich shell can protect the Ni-rich core from electrolyte attack as well as the Ni-rich core maintains a high and stable average voltage [27,32]. Li et al. reported that reducing the Co content can significantly suppress voltage attenuation [33]. Therefore, it is very important indication for Li-rich layered oxide cathode material to control the composition of TM ions in the $LiMO_2$ layer in order to suppress the voltage attenuation.

To further investigate the effect of different compositions in the $LiMO_2$ layer on the physicochemical properties of Li-rich layered oxide cathode materials, we synthesize LL-111, LL-523 and LL-811 cathode materials by means of solid-state complexation method, and the electrochemical properties have been investigated. During these three composition samples, LL-811 exhibits slower voltage decay and more excellent cycle stability during long-term cycling. The capacity retention rate of the LL-811 is 87.5% at 1C rate after 100 cycles, and its voltage attenuation is quite low with 0.460 V. The distinctive advantage of this LL-811 Li-rich cathode material may derive from the high nickel content in the layered (R-3m) phase. High-nickel-content Li-rich layered oxide cathode material may cause more Ni^{2+} ions to occupy the Li^+ ion sites in the lithium layer, It can result in a part of nickel to be doped at Li^+ ion sites [34]. The cation doping, to some extent, can improve the structural stability by supporting the Li slabs and reducing tension of neighboring oxygen layers during the delithiation process [23]. In addition, nickel acts as a stabilizer to reduce the complete transformation of manganese by substitution. The preferential reduction of $Ni^{4+/2+}$ maintains average oxidation state of Mn above 3+, as well as suppresses the Jahn−Teller effect caused by Mn^{3+} ions and effectively improves structural durability [35-37].

2. Materials and Methods

2.1. Sample preparation

The $0.5Li_2MnO_3 \cdot 0.5LiNi_{1-x-y}Co_xMn_yO_2$ (x=0.33, 0.1, 0.2; y=0.33, 0.1, 0.3.) cathode materials (marked as LL-111, LL-523, LL-811, respectively.) were synthesized by a solid-sate complexation method using citric acid monohydrate as complexing agent with analytical grade chemicals $LiAc \cdot 2H_2O$ (Excess 5%,AR, 99%), $Ni(Ac)_2 \cdot 4H_2O$ (AR, 98%), $Co(Ac)_2 \cdot 4H_2O$ (AR, 99.5%), $Mn(Ac)_2 \cdot 4H_2O$ (AR, 99%), citric acid monohydrate (AR, 99.5%). The molar ratio between transition metal ion and citric acid monohydrate was 1:1. Using a certain amount of absolute ethanol as a solvent, a stoichiometric amount of above reagents were mixed thoroughly and ball milled at the speed of 200 rpm continuously for 4 h. After ball milling, it was dried in an oven at 80 ℃ for 24 h in order to get a uniform mixed precursor. The precursor was ball milled for 30 min and precalcined at 450 ℃ for 6 h in air to eliminate the organic substancesand then was cancined at 900 ℃, 900 ℃, 800 ℃ for 12 h in air at the rate of 5 $℃ \cdot min^{-1}$, respectively. And finally these required samples were obtained.

2.2. Materials Characterizations

The crystallographic structure $0.5Li_2MnO_3 \cdot 0.5LiNi_{1-x-y}Co_xMn_yO_2$ (LL-111, LL-523, LL-811) cathode materilas were carried out by X-ray diffraction (XRD, Bruker D8) with Cu Kα radiation(λ = 1.54056Å) in the range of 10°-90° with the speed of 5° min^{-1}. The microscopic morphology was investigated with scanning electron microscopy (SEM, TESCAN MIRA3 LMU) and transmission electron microscopy (TEM, Tecnai G2 F20).

Electrochemical performance of the samples were characterized using galvanostatic charge-discharge tests with two-electrode coin cells (type CR-2025).The synthesized sample, acetylene black and polyvinylidene difluoride (PVDF) with a weight ratio of 8:1:1 to make a slurry in the N-

Peer-reviewed version available at *Materials* **2019**, *13*, 40; doi:10.3390/ma13010040

methylpyrrolidone (NMP) solvent. The slurry was uniformly coated onto aluminum foil as current collector and then dried at 120 ℃ for 6 h under vacuum oven. Cells were assembled in an Argon-filled glove box with H_2O and O_2 contents below 0.01 ppm, using the metallic lithium foil as an anode. The electrolyte was 1 M LiPF6 dissolved in ethyl carbonate (EC) and dimethyl carbonate (DMC) (1:1 in volume) and the separator was Cellgard 2500 membrane.

The Galvanostatic charge-discharge measurements were carried out using NEWARE CT-4008 battery testing system (Shenzhen, China) within the voltage range of 2.0–4.8 V at 25 ℃. Cyclic voltammetry (CV) and AC impedance (EIS, 1mHz-0.1MHz) using a CHI660E electrochemical workstation (Shanghai, China).

3. Results and discussion

3.1. Crystal structure and microstructure

Using citric acid monohydrate as complexing agent, the $0.5Li_2MnO_3\cdot 0.5LiNi_{1-x-y}Co_xMn_yO_2$ cathode materials (LL-111, LL-523, LL-811) were synthesized by a solid-state complexation method. The phase and crystal structure of the above cathode materials were respectively analyzed by XRD. The XRD patterns of the sample LL-111, LL-523, LL-811 are shown in Figure 1. Using the JADE 6.5 analysis software to analyze the XRD datas, the diffraction peaks of three samples can be indexed to a typical α-$NaFeO_2$ structure (R-3m) and the enlargements of the small region from 20 to 24° are attributed to Li_2MnO_3 phase (C2/m) [38-39]. Complete splitting of the two pair diffraction peaks (006)/(102) and (018)/(110) indicates the integrity of the layered structure for all samples. It is noted that, the intensity of Li_2MnO_3 characteristic peak gradually decreases with the metallic nickel content increasing.

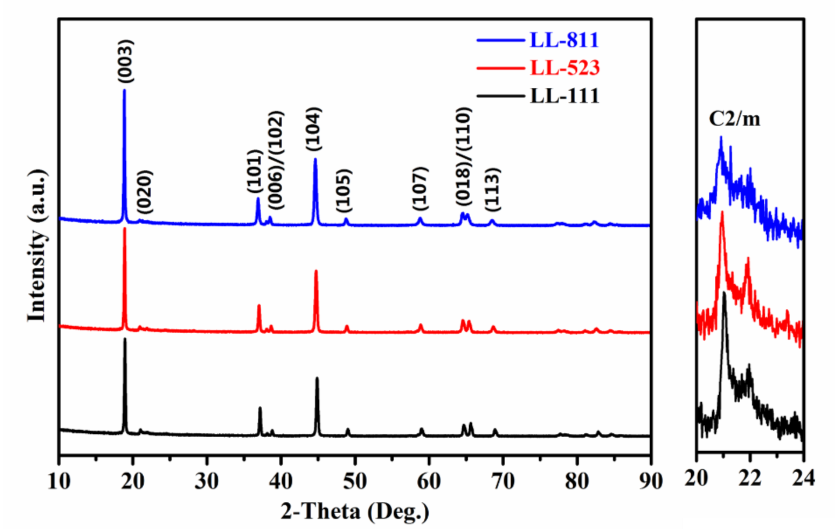

Figure 1. XRD patterns of LL-111, LL-523, LL-811, which adopts a α-$NaFeO_2$ structure. The XRD patterns on the right show the enlargement of Li_2MnO_3 characteristic peak over a small 2θ region.

The surface morphologies of LL-111, LL-523, LL-811 samples and corresponding element compositions are shown in Figure 2. As seen in Figue 2a-2c, three samples shows irregular polyhedral morphology with a size of approximately 200-500 nm, which is consistent with previous literatures [6,40-41]. In Figure 2a, LL-111 particles show better dispersion and smooth surface. As the nickel content increases, particle agglomeration becomes more and more seriously. Besides, the interface between the particles is blurred and even disappears. As seen in Figure 2d-2e, the actual ratios of LL-811 and LL-523, LL111 cathode materials are basically in accordance with the designed values. However, LL-811 (Figure 2f) shows a Mn-rich trend on the surface, which may be mainly due to the concentration gradient of Ni/Mn with the nickel content increasing.

Peer-reviewed version available at *Materials* **2019**, *13*, 40; doi:10.3390/ma13010040

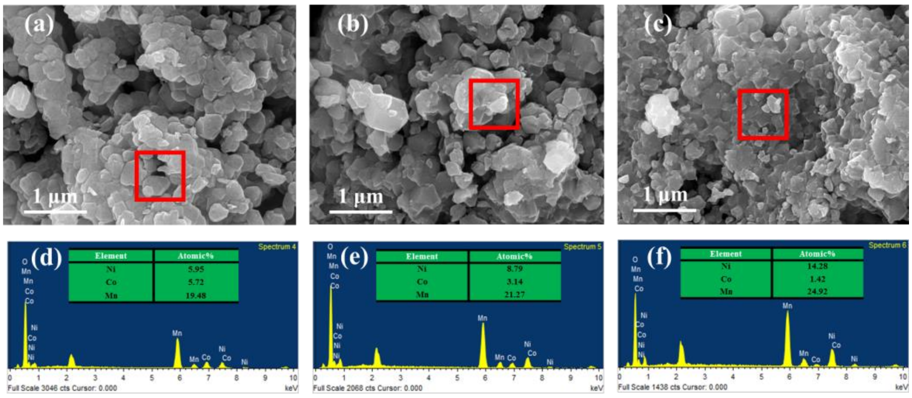

Figure 2. SEM images of (a) LL-111, (b) LL-523, (c) LL-811; Elemental mapping images (d–f) of LL-111, LL-523, LL-811 respectively.

To explore the precise structural properties of Li-rich cathode materials with high nickel content, TEM and HRTEM images are shown in Figure 3. As seen in Figure 3a and 3d, the edge of LL-811 cathode material is smooth and evenly distributed. Besides, it has relatively straight and continuous lattice fringes, and the interplanar spacing of (003) crystal plane is 4.72**Å** (Figure 3b), which shows the characteristics of good layered structure material (FFT results in insets of Figure 3c). The lattice fringes of Figure 3e show a distinct two-phase composite (FFT results in insets of Figure 3f). As clearly seen in Figure 3g, the internal phase distribution of the bulk is not very uniform, and Figure 3h further verifies this phenomenon. Figure 3h and FFT results show three kinds of different plane spaces and crystal plane orientations, which represent the (003) crystal plane of the LL-811 structure (4.72Å), the (006) crystal plane of the LL-811 structure (2.36Å), two-phase (Li_2MnO_3 and $LiMO_2$) composite, respectively.

In order to further verify the elemental uniformity of the LL-811 sample, an EDX linear scanning of the single particle was carried out in Figure 4a-4b. A very important message can be obtained from Figure 4b, in which the content of Mn element gradually increases from internal to external and Mn-rich phase appears on the surface. However the change trend of nickel element is opposite, which may be mainly due to the segregation of Mn and Ni elements. Nickel has high catalytic activity and is easy to react with electrolyte, while Mn-rich on the surface can effectively inhibit the reaction. The Mn-rich surface phenomenon may explain the excellent prolong cycling stability of LL-811 cathode materials [25,27].

Peer-reviewed version available at *Materials* **2019**, *13*, 40; doi:10.3390/ma13010040

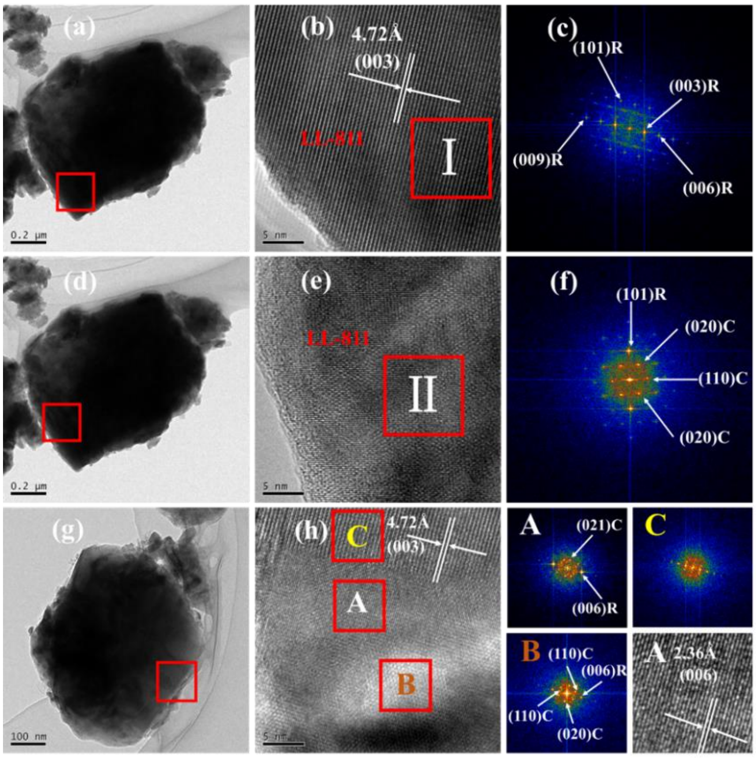

Figure 3. TEM images: (a), (d) and (g), HRTEM images: (b), (e) and (h) of different regions of LL-811 and corresponding the Fourier transform (FFT) images of each region.

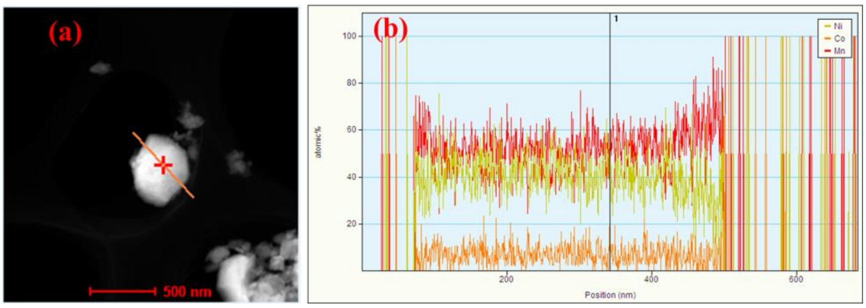

Figure 4. TEM images: (a), (b) EDX linear scanning analysis of of LL-811 individual particles and corresponding the linear scanning.

3.2. Electrochemical charge/discharge behavior

In order to evaluate the electrochemical property of the samples LL-111, LL-523 and LL-811, the first charge-discharge curves, rate performances from 0.1C to 5C and cycling performances at 1C (1C=200 mAh·g^{-1}) between 2 V to 4.8 V are shown in Figure 5. As shown in Fig 5a, there are two distinct voltage plateaus during the first charge process: (1) a smooth voltage plateau below 4.5 V and (2) a long voltage plateau about 4.5 V [42]. The first discharge capacities of LL-111, LL-523, LL-811 are 284.6 mAh·g^{-1}, 263.0 mAh·g^{-1}, 207.4 mAh·g^{-1}, respectively. The ionic radius of Ni^{2+} (0.70Å) is similar with Li^{+} (0.76Å), so it could result in some nickel ions occupying lithium sites as the nickel content increases.

LL-111 samples at 1C delivers 206.4 mAh·g^{-1} and about 98.5% of the capacity is maintained even after 100 cycles. The first discharge capacity of LL-523 at 1C is 194.1 mAh·g^{-1} and about 80.0% of the capacity is maintained after 100 cycles. In contrast to LL-111 and LL-523, the capacity retention of the LL-811 is 87.5% after 100 cycles, although the first discharge capacity of LL-811 at 1C only is 154.6 mAh·g^{-1}. By comparison, the cycle stability of the high-nickel-content LL-811 cathode material is more excellent. It can be attributed to that nickel ions easily migrate out of the TM layer to support the structure instead of being trapped in the middle tetrahedral layer [23].

Figure 5c shows the rate performance of these three samples at different current densities of 0.1C, 0.2C, 0.5C, 1C, 3C, 5C at 25 ℃ between 2 V and 4.8 V. As seen in Figure 5c, the discharge capacities of LL-111, LL-523 and LL-811 are 130.8 mAh·g^{-1}, 118.9 mAh·g^{-1} and 100.5 mAh·g^{-1}, respectively at 5C. The low rate capacity is ascribed to the sluggish kinetics of high nickel cathode materials. After EIS measurement, the Li$^+$ diffusion coefficient of LL-111, LL-523 and LL-811 three samples is 2.77×10^{-14} cm^2 S^{-1}, 3.70×10^{-14} cm^2 S^{-1} and 1.32×10^{-14} cm^2 S^{-1}, respectively. Moreover, as seen in Fig 5f, the charge transfer impedance (R_{ct}) is 212 Ω, 352 Ω and 606.7 Ω for the LL-111, LL-523 and LL-811 samples. The R_{ct} of high nickel LL-811 cathode material is very large compared to the other two samples, which can be attributed to the low electronic conductivity.

The most striking performance feature of LL-811 cathode materials is its low voltage attenuation after prolong cycling. Figure 5d shows the relationship between the average voltage and cycle number. The voltage attenuation is approximately 0.460 V after 100 cycles at 1 C, while for LL-111 and LL-523, the voltage attenuation is reached up to 0.665 V and 0.600 V, respectively.

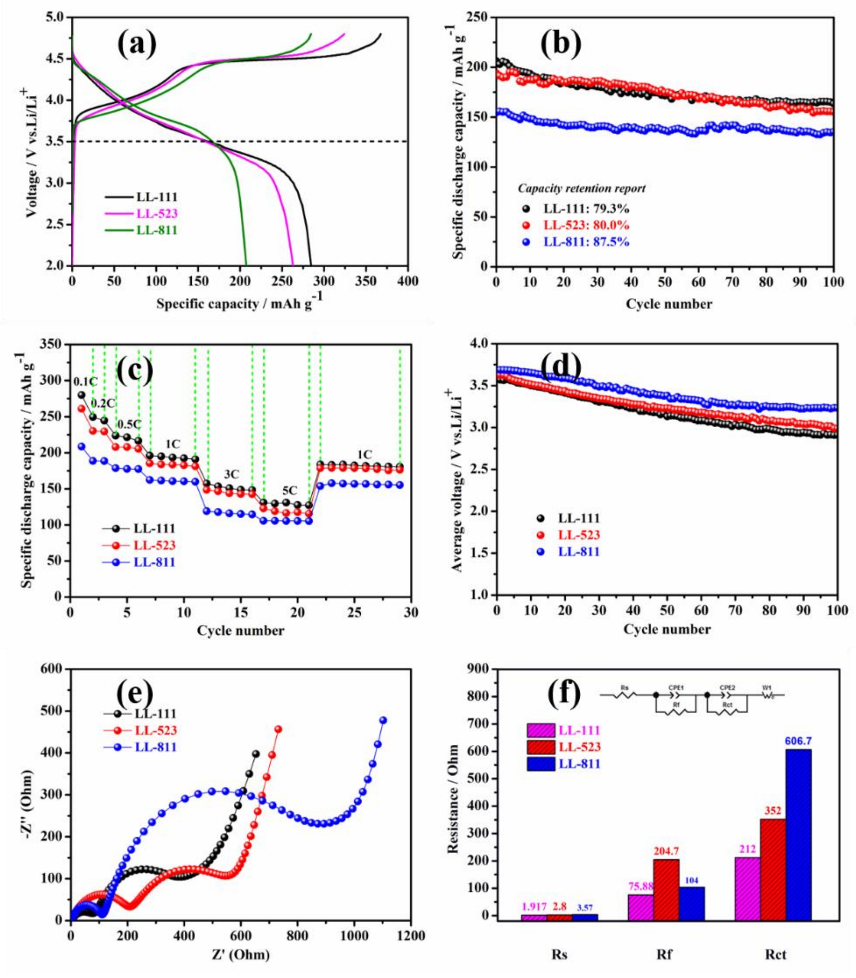

Figure 5. Electrochemical performances: (a) First charge- discharge curves at 0.1C; (b) The cycle performances at 1C; (c) The rate performances from 0.1C to 5C; (d) Average voltage attenuation curves after 100 cycles at 1C; Nyquist plots: (e) fresh cells; (f) Fitted impedance data of LL-111, LL-523 and LL-811 cells between 2 V to 4.8 V.

To further illustrate the voltage attenuation phenomenon of Li-rich cathode materials upon cycling, discharge curves with different cycles between 2 V to 4.8 V at 1C and cyclic voltammetry (CV) curves of LL-111, LL-523 and LL-811 are shown in Figure 6. As seen in Figure 6(a, b, c), voltage attenuates rapidly at 1C for LL-111, and for LL-523 it is slower than LL-111, whereas for LL-811 it is the lowest. Figure 6(d, e, f) clearly characterize that the three samples display distinct oxidation peaks appeared at 4.0 V during the first cycle, corresponding to the oxidation reactions of Ni$^{2+/3+/4+}$ and Co$^{3+/4+}$; and the oxidation peak at 4.6 V corresponds to the activation process of Li_2MnO_3 [43]. The reduction peaks at 3.3 V, 3.6 V, 4.1 V reflect Mn$^{4+/3+}$, Ni$^{4+/3+}$, Co$^{4+/3+}$ [44], respectively. By comparison, as seen clearly in Figure 6(d, e, f), the voltage decay is minimal for LL-811 after 3 cycles, which is consistent with the phenomenon observed with the voltage attenuation curves. LL-111 and LL-523 Li-rich materials suffers from voltage attenuation after prolong cycling, especially LL-111, for which its capacity mainly came from the low voltage region [23]. Therefore the specific energy (specific energy = specific capacity × average voltage) output of the battery further lowered upon cycling owing to the disappointing cycle stability and severe voltage attenuation for LL-111 and LL-523 cathode materials. This is due to the phase transformation from layered to spinel-like or rock-salt phases during repeated charge and discharge cycles. Comparing with LL-111 and LL-523 (64.6% and 67.0% energy retention after 100 cycles, respectively), the specific energy retention was 76.7% for LL-811 after 100 cycles. The excellent cell properties of LL-811 indicate that increasing the nickel content could significantly inhibit the intrinsic voltage attenuation of Li-rich materials. These consequences demonstrate that high-nickel-content Li-rich cathode materials, such as LL-811, exhibit outstanding structural durability during prolong cycling, which will promote the commercialization of Li-rich cathode materials.

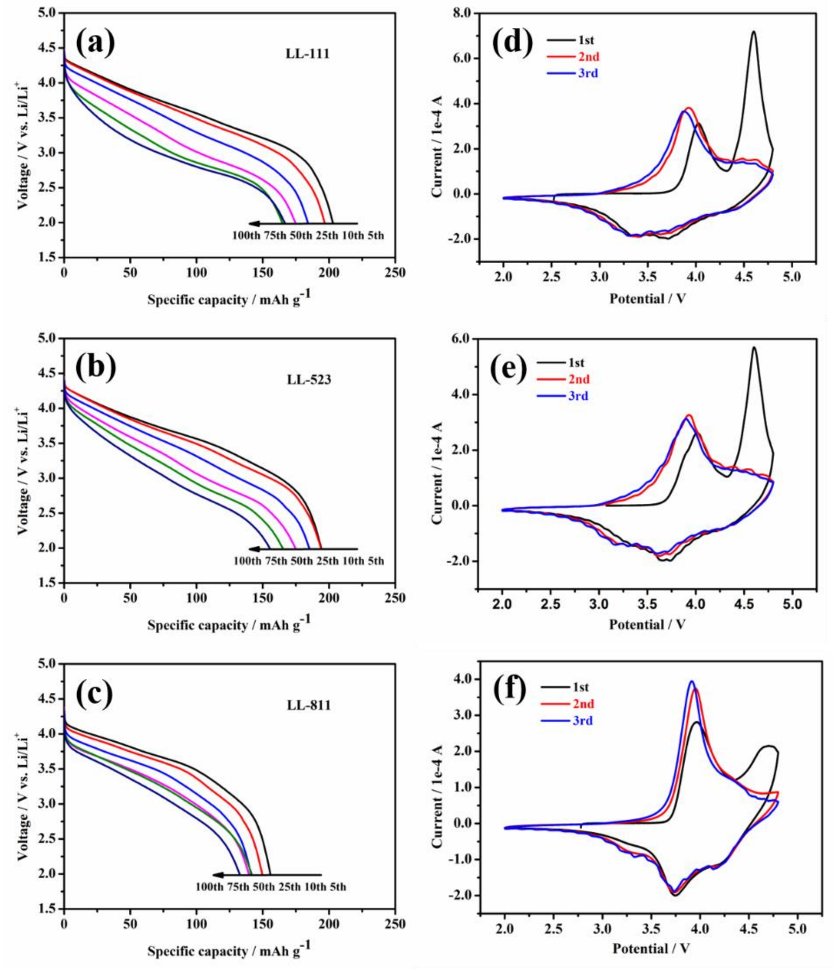

Figure 6. Discharge curves with different cycles between 2 V to 4.8 V at 1C and Cyclic Voltammetry (CV) curves of LL-111 (a, d), LL-523 (b, e) and LL-811 (c, f).

To further assess the effect of nickel content on the structural durability of Li-rich cathode materials, the XRD patterns of LL-111, LL-523 and LL-811 electrodes after 100 cycles are shown in Figure 7. The intensity ratios of both the (003) and (104) peaks of LL-111, LL-523 and LL-811 are shown in Table 1. Compared to LL-111 and LL-523, the intensity ratio of the (003) and (104) peaks of the LL-811 cathode material is still greater than 1.2 after 100 cycles [45-46], which indicates that the high

Peer-reviewed version available at *Materials* **2019**, *13*, 40; doi:10.3390/ma13010040

nickel cathode materials can maintain their structural durability and inhibit the phase transformation to a certain degree during prolong cycling.

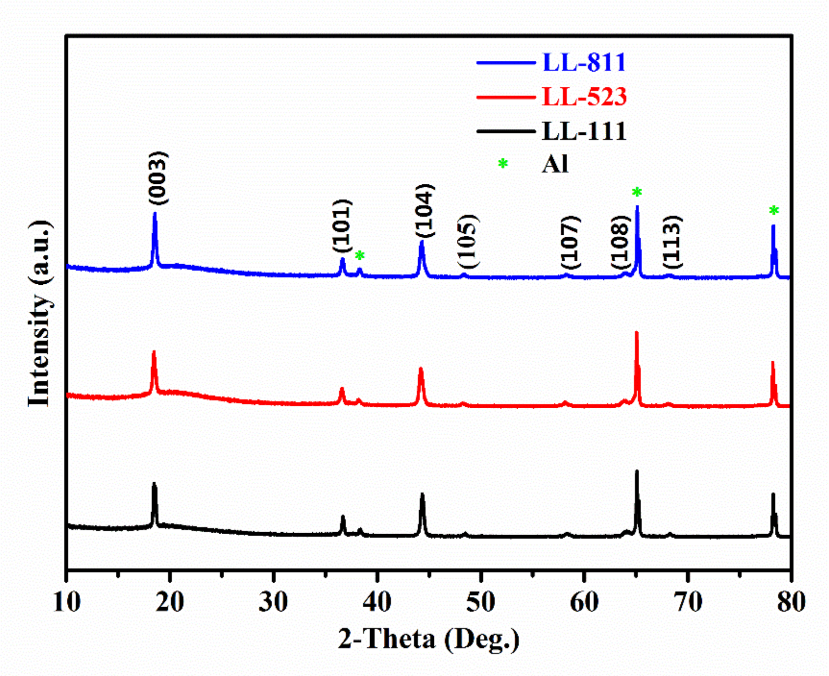

Figure 7. XRD patterns of LL-111, LL-523 and LL-811 electrodes after 100 cycles.

Table 1. The ratios $I_{(003)}$ /$I_{(104)}$ of LL-111, LL-523 and LL-811 samples before and after cycling by calculating from the XRD data.

Samples	Before cycling	After cycling
LL-111	1.6628	1.2285
LL-523	1.6751	1.4190
LL-811	2.0120	1.7083

4. Conclusions

In this paper, LL-111, LL-523 and LL-811 cathode materials were successfully synthesized by a solid-sate complexation method using citric acid monohydrate as complexing agent. Compared to the LL-111 and LL-523, the high-nickel-content LL-811 cathode material shows an excellent cycling stability (capacity retention of 87.5% at 1C rate after 100 cycles) and suppresses voltage attenuation (only 0.460 V after 100 cycles) during prolong cycling. This proves that it is very important for Li-rich layered oxide cathode materials to control the composition of TM ions in the $LiMO_2$ layer. This further demonstrates that the nickel content plays a very important role in stabilizing the structure and suppressing the voltage decay. This paper promotes effect of different components on voltage attenuation of Li-rich cathode materials, especially the nickel content, which is of great reference and guiding significance for the practical application of Li-rich layered oxide cathode materials.

Author Contributions: Methodology and Conceptualization, Z.C., J.L. and Q.L.; resources, Z.C. and H.Z.; data curation, Y.J., B.L., J.L. and F.L.; writing—original draft preparation, J.L.; writing—review and editing, Q.L., L.J. and J.D.; funding acquisition, Z.C. and H.Z.

Funding: This work was supported by the National Natural Science Foundation of China (No. 51874048), the National Science Foundation for Young Scientists of China (No. 51604042), the Research Foundation of Education Bureau of Hunan Province (No.19A003) and Scientific Research Fund of Changsha Science and Technology Bureau (No. kq1901100) and Postgraduate Innovative Test Program of Hunan Province.

Peer-reviewed version available at *Materials* **2019**, *13*, 40; doi:10.3390/ma13010040

Conflicts of Interest: The authors declare no conflict of interest.

References

1. Li, J.F.; Li, M.; Zhang, L.; Wang, J.Z. General synthesis of $xLi_2MnO_3\cdot(1-x)LiNi_{1/3}Co_{1/3}Mn_{1/3}O_2$ (x = 1/4, 1/3, and 1/2) hollow microspheres towards enhancing the performance of rechargeable lithium ion batteries. *Journal of Materials Chemistry A* **2016,** *4*, 12442-12450.
2. Chen, Z.Y.; Yan, X.Y.; Xu, M.; Cao, K.F.; Zhu, H.L.; Li, L.J.; Duan, J.F. Building Honeycomb-Like Hollow Microsphere Architecture in a Bubble Template Reaction for High-Performance Lithium-Rich Layered Oxide Cathode Materials. *ACS Appl Mater Interfaces* **2017,** *9*, 30617-30625.
3. Yang, H.P.; Wu, H.H.; Ge, M.Y.; Li, L.J.; Yuan, Y.F.; Yao, Q.; Chen, J.; Xia, L.F.; Zheng, J.M.; Chen, Z.Y.; Duan, J.F.; Kisslinger, K.; Zeng, X.C.; Lee, W.K.; Zhang, Q.B.; Lu, J. Simultaneously Dual Modification of Ni-Rich Layered Oxide Cathode for High-Energy Lithium-Ion Batteries. *Advanced Functional Materials* **2019,** *29*, 1808825-1808837.
4. Whittingham, M.S. Lithium Batteries and Cathode Materials. *Chemical Reviews* **2004,** *104*, 4271-4302.
5. Armand, M.; Tarascon, J. M. Building better batteries. *Nature* **2008,** *451*, 652-657.
6. Xu, M.; Chen, Z.Y.; Li, L.J.; Zhu, H.L.; Zhao, Q.F.; Xu, L.; Peng, N.F.; Gong, Li. Highly crystalline alumina surface coating from hydrolysis of aluminum isopropoxide on lithium-rich layered oxide. *Journal of Power Sources* **2015,** *281*, 444-454.
7. Hu, B.; Lou, X.B.; Li, C.; Geng, F.S.; Zhao, C.; Wang, J.Y.; Shen, M.; Hu, B.W. Reversible phase transition enabled by binary Ba and Ti-based surface modification for high voltage $LiCoO_2$ cathode. *Journal of Power Sources* **2019,** *438*, 226954-226961.
8. Choi, J.W.; Aurbach, D. Promise and reality of post-lithium-ion batteries with high energy densities. *Nature Reviews Materials* **2016,** *1*, 1-16.
9. Huang, W.; Wang, G.; Luo, C.; Xu, Y.B.; Xu, Y.; Ecksteina, B.J.; Chen, Y.; Wang, B.H.; Huang, J.X.; Kang, Y.J.; Wu, J.S.; Dravid, V.P.; Facchetti, A.; Marks, T.J. Controllable growth of $LiMn_2O_4$ by carbohydrate-assisted combustion synthesis for high performance Li-ion batteries. *Nano Energy* **2019,** *64*, 103936-103945.
10. Wang, Y.H.; Wang, Y.H.; Jia, D.S.; Peng, Z.; Xia, Y.Y.; Zheng, G.F. All-nanowire based Li-ion full cells using homologous Mn_2O_3 and $LiMn_2O_4$. *Nano Letters* **2014,** *14*, 1080-1084.
11. Gu, L.; Zhu, C.B.; Li, H.; Yu, Y.; Li, C.L.; Tsukimoto, S.; Maier, J.; Ikuhara, Y. Direct observation of lithium staging in partially delithiated $LiFePO_4$ at atomic resolution. *Journal of the American Chemical Society* **2011,** *133*, 4661-4663.
12. Zhao, Y.; Peng, L.L.; Liu, B.R.; Yu, G.H. Single-crystalline $LiFePO_4$ nanosheets for high-rate Li-ion batteries. *Nano Letters* **2014,** *14*, 2849-2853.
13. Myung, S.T.; Maglia, F.; Park, K.J.; Yoon, C.S.; Lamp, P.; Kim, S.J.; Sun, Y.K. Nickel-Rich Layered Cathode Materials for Automotive Lithium-Ion Batteries: Achievements and Perspectives. *ACS Energy Letters* **2016,** *2*, 196-223.
14. Yang, H.; Du, K.; Hu, G.R.; Peng, Z.D.; Cao, Y.B.; Wu, K.P.; Lu, Y.; Qi, X.Y.; Mu, K.C.; Wu, J.L. Graphene@TiO_2 co-modified $LiNi_{0.6}Co_{0.2}Mn_{0.2}O_2$ cathode materials with enhanced electrochemical performance under harsh conditions. *Electrochimica Acta* **2018,** *289*, 149-157.
15. Chen, Z.Y.; Gong, X.L.; Zhu, H.L.; Cao, K.F.; Liu, Q.M.; Liu, J.; Li, L.J.; Duan, J.F. High Performance and Structural Stability of K and Cl Co-Doped $LiNi_{0.5}Co_{0.2}Mn_{0.3}O_2$ Cathode Materials in 4.6 Voltage. *Front Chem* **2018,** *6*, 643-668.
16. Chen, Z.Y.; Cao, K.F.; Zhu, H.L.; Li, L.J.; Gong, X.L.; Liu, Q.M.; Duan, J.F. Improved Electrochemical Performance of Surface Coated $LiNi_{0.80}Co_{0.15}Al_{0.05}O_2$ With Polypyrrole. *Front Chem* **2018,** *6*, 648-657.
17. Yabuuchi, N.; Yoshii, K.; Myung, S.T.; Nakai, I.; Komaba, S. Detailed studies of a high-capacity electrode material for rechargeable batteries, Li_2MnO_3-$LiCo_{1/3}Ni_{1/3}Mn_{1/3}O_2$. *Journal of the American Chemical Society* **2011,** *133*, 4404-4419.
18. Ma, Y.T.; Liu, P.F.; Xie, Q.S; Zhang, G.B.; Zheng, H.F.; Cai, Y.X.; Li, Z.; Wang, L.S.; Zhu, Z.Z.; Mai, L.Q.; Peng, D.L. Double-shell Li-rich layered oxide hollow microspheres with sandwich-like carbon@spinel@layered@spinel@carbon shells as high-rate lithium ion battery cathode. *Nano Energy* **2019,** *59*, 184-196.
19. Qing, R.P.; Shi, J.L.; Xiao, D.D.; Zhang, X.D.; Yin, Y.X.; Zhai, Y.B.; Gu, L.; Guo, Y.G. Enhancing the Kinetics of Li-Rich Cathode Materials through the Pinning Effects of Gradient Surface Na^+ Doping. *Advanced Energy Materials* **2016,** *6*, 1501914-1501919.

20. Ning, F.H.; Shang, H.F.; Li, B.; Jiang, N.; Zou, R.Q.; Xia, D.G. Surface thermodynamic stability of Li-rich Li_2MnO_3: Effect of defective graphene. *Energy Storage Materials* **2019**, *22*, 113-119.
21. Yan, P.F.; Nie, A.M.; Zheng, J.M.; Zhou, Y.G.; Lu, D.P.; Zhang, X.F.; Xu, R.**;** Belharouak, I.; Zu, X.T.; Xiao, J.; Amine, K.; Liu, J.; Gao, F.; Reza S.Y, Zhang, J.G.; Wang. C.M. Evolution of lattice structure and chemical composition of the surface reconstruction layer in $Li_{1.2}Ni_{0.2}Mn_{0.6}O_2$ cathode material for lithium ion batteries. *Nano Letters* **2015**, *15*, 514-522.
22. Liu, Y.Y.; Li, R.R; Li, J.L.; Yang, Z.; Zhong, J.J.; Wang, Z.; Kang, F.Y. A high-performance Ce and Sn co-doped cathode material with enhanced cycle performance and suppressed voltage decay for lithium ion batteries. *Ceramics International* **2019**, *45*, 20780-20787.
23. Shi, J.L.; Zhang, J.N.; He, M.; Zhang, X.D.; Yin, Y.X.; Li, H.; Guo, Y. G.; Gu, L.; Wan, L.J. Mitigating Voltage Decay of Li-Rich Cathode Material via Increasing Ni Content for Lithium-Ion Batteries. *ACS Appl Mater Interfaces* **2016**, *8*, 20138-20146.
24. Xu, M.; Chen, Z.Y.; Zhu, H.L.; Yan, X.Y.; Li, L.J.; Zhao, Q.F. Mitigating capacity fade by constructing highly ordered mesoporous Al_2O_3/polyacene double-shelled architecture in Li-rich cathode materials. *Journal of Materials Chemistry A* **2015**, *3*, 13933-13945.
25. Ju, X.K.; Hou, X.; Liu, Z.Q.; Zheng, H.F.; Huang, H.; Qu, B.H.; Wang, T.H.; Li, Q.H.; Li, J. The full gradient design in Li-rich cathode for high performance lithium ion batteries with reduced voltage decay. *Journal of Power Sources* **2019**, *437*, 226902-226910.
26. Gu, M.; Genc, A.; Belharouak, I.; Wang, D.P.; Amine, K.; Thevuthasan, S.; Baer, D.R.; Zhang, J.G.; Browning, N.D.; Liu, J.; Wang, C.M. Nanoscale Phase Separation, Cation Ordering, and Surface Chemistry in Pristine $Li_{1.2}Ni_{0.2}Mn_{0.6}O_2$ for Li-Ion Batteries. *Chemistry of Materials* **2013**, *25*, 2319-2326.
27. Li, J.; Camardese, J.; Shunmugasundaram, R.; Glazier, S.; Lu, Z.G.; Dahn, J.R. Synthesis and Characterization of the Lithium-Rich Core–Shell Cathodes with Low Irreversible Capacity and Mitigated Voltage Fade. *Chemistry of Materials* **2015**, *27*, 3366-3377.
28. Sathiya, M.; Abakumov, A.M.; Foix, D.; Rousse, G.; Ramesha, K.; Saubanère, M.; Doublet, M. L; Vezin, H.; Laisa, C.P.; Prakash, A.S.; Gonbeau, D.; VanTendeloo, G.; Tarascon, J.M. Origin of voltage decay in high-capacity layered oxide electrodes. *Nature Materials* **2014**, *14*, 230-238.
29. Boulineau, A.; Simonin, L.; Colin, J.F.; Canévet, E.; Daniel, L.; Patoux, S. Evolutions of $Li_{1.2}Mn_{0.61}Ni_{0.18}Mg_{0.01}O_2$ during the Initial Charge/Discharge Cycle Studied by Advanced Electron Microscopy. *Chemistry of Materials* **2012**, *24*, 3558-3566.
30. Wu, F.; Li, N.; Su, Y.F.; Zhang, L.J.; Bao, L.Y.; Wang, J.; Chen, L.; Zheng, Y.; Dai, L.Q.; Peng, J.Y.; Chen, S. Ultrathin spinel membrane-encapsulated layered lithium-rich cathode material for advanced Li-ion batteries. *Nano Letters* **2014**, *14*, 3550-3555.
31. Li, H.Y.; Cormier, M.; Zhang, N.; Inglis, J.; Li, J.; Dahn, J.R. Is Cobalt Needed in Ni-Rich Positive Electrode Materials for Lithium Ion Batteries? *Journal of The Electrochemical Society* **2019**, *166*, A429-A439.
32. Kim, U.H.; Kim, J.H.; Hwang, J.Y.; Ryu, H.H.; Yoon, C.S.; Sun, Y.K. Compositionally and structurally redesigned high-energy Ni-rich layered cathode for next-generation lithium batteries. *Materials Today* **2019**, *23*, 26-36.
33. Wang, J.; He, X.; Paillard, E.; Laszczynski, N.; Li,J.; Passerini, S. Lithium- and Manganese-Rich Oxide Cathode Materials for High-Energy Lithium Ion Batteries. *Advanced Energy Materials* **2016**, *6*, 1600906-1600922.
34. Shi, J.L.; Xiao, D.D.; Ge, M.; Yu, X.; Chu, Y.; Huang, X.; Zhang, X.D.; Yin, Y.X.; Yang, X.Q.; Guo, Y.G.; Gu, L.; Wan, L.J. High-Capacity Cathode Material with High Voltage for Li-Ion Batteries. *Adv Mater* **2018**, *30*, 1705575-1705582.
35. Hy, S.; Cheng, J.H.; Liu, J.Y.; Pan, C.J.; Rick, J.; Lee, J.F.; Chen, J.M.; Hwang, B.J. Understanding the Role of Ni in Stabilizing the Lithium-Rich High-Capacity Cathode Material $Li[Ni_xLi_{(1-2x)/3}Mn_{(2-x)/3}]O_2 (0 \leq x \leq 0.5)$. *Chemistry of Materials* **2014**, *26*, 6919-6927.
36. Kim, T.; Song, B.H.; Lunt, A.G.; Cibin, G.; Dent, A.J.; Lu, L.; Korsunsky, A.M. In operando X-ray absorption spectroscopy study of charge rate effects on the atomic environment in graphene-coated Li-rich mixed oxide cathode. *Materials & Design* **2016**, *98*, 231-242.
37. Yang, F.; Zhang, Q.G.; Hu, X.H.; Peng, T.Y.; Liu, J.Q. Preparation of Li-rich layered-layered type $xLi_2MnO_3{\cdot}(1-x)LiMnO_2$ nanorods and its electrochemical performance as cathode material for Li-ion battery. *Journal of Power Sources* **2017**, *353*, 323-332.

Peer-reviewed version available at *Materials* **2019**, *13*, 40; doi:10.3390/ma13010040

38. Yan, P.F.; Xiao, L.; Zheng, J.M.; Zhou, Y.G.; He, Yang; Z., X.T.; Mao, S.X.; Xiao, J.; Gao, F.; Zhang, J.G.; Wang, C.M. Probing the Degradation Mechanism of Li2MnO3Cathode for Li-Ion Batteries. *Chemistry of Materials* **2015,** *27*, 975-982.
39. Wang, P.B.; Luo, M.Z.; Zheng, J.C.; He, Z.J.; Tong, H.; Yu, W.J. Comparative Investigation of $0.5Li_2MnO_3.0.5LiNi_{0.5}Co_{0.2}Mn_{0.3}O_2$ Cathode Materials Synthesized by Using Different Lithium Sources. *Front Chem* **2018,** *6*, 159-167.
40. Zhang, L.J.; Wu, B.R.; Li, N.; Wu, F. Hierarchically porous micro-rod lithium-rich cathode material $Li_{1.2}Ni_{0.13}Mn_{0.54}Co_{0.13}O_2$ for high performance lithium-ion batteries. *Electrochimica Acta* **2014,** *118*, 67-74.
41. Zhou, L.Z.; Xu, Q.J.; Liu, M.S.; Jin, X. Novel solid-state preparation and electrochemical properties of $Li_{1.13}[Ni_{0.2}Co_{0.2}Mn_{0.47}]O_2$ material with a high capacity by acetate precursor for Li-ion batteries. *Solid State Ionics* **2013,** *249-250*, 134-138.
42. Yang, S.Q.; Wang, P.B.; Wei, H.X.; Tang, L.B.; Zhang, X.H.; He, Z.J.; Li, Y.J.; Tong, H.; Zheng, J.C. $Li_4V_2Mn(PO_4)_4$-stablized $Li[Li_{0.2}Mn_{0.54}Ni_{0.13}Co_{0.13}]O_2$ cathode materials for lithium ion batteries. *Nano Energy* **2019,** *63*, 103889-103898.
43. Zuo, Y.X.; Li, B.; Jiang, N.; Chu, W.S.; Zhang, H.; Zou, R.Q.; Xia, D.G. A High-Capacity O2-Type Li-Rich Cathode Material with a Single-Layer Li_2MnO_3 Superstructure. *Adv Mater* **2018,** *30*, 1707255-1707259.
44. Xiong, F.Y.; Tan, S.H.; Wei, Q.L.; Zhang, G.B.; Sheng, J.Z.; An, Q.Y.; Mai, L.Q. Three-dimensional graphene frameworks wrapped $Li_3V_2(PO_4)_3$ with reversible topotactic sodium-ion storage. *Nano Energy* **2017,** *32*, 347-352.
45. Liu, J.L.; Chen, L.; Hou, M.Y.; Wang, F.; Che, R.C.; Xia, Y.Y. General synthesis of $xLi_2MnO_3\cdot(1-x)LiMn_{1/3}Ni_{1/3}Co_{1/3}O_2$ nanomaterials by a molten-salt method: towards a high capacity and high power cathode for rechargeable lithium batteries. *Journal of Materials Chemistry* **2012,** *22*, 25380-25387.
46. Yang, X.K.; Wang, D.; Yu, R.Z.; Bai, Y.S.; Shu, H.B.; Ge, L.; Guo, H.P.; Wei, Q.L.; Liu, L.; Wang, X.Y. Suppressed capacity/voltage fading of high-capacity lithium-rich layered materials via the design of heterogeneous distribution in the composition. *Journal of Materials Chemistry A* **2014,** *2*, 3899-3911.